Scratching as a Fracture Process: From Butter to Steel

A-T. Akono,[1] P. M. Reis,[1,2] and F-J. Ulm[1,*]

[1]Department of Civil and Environmental Engineering, Massachusetts Institute of Technology, Cambridge, Massachusetts 02139, USA
[2]Department of Mechanical Engineering, Massachusetts Institute of Technology, Cambridge 02139, USA

(Received 8 December 2010; published 20 May 2011)

We present results of a hybrid experimental and theoretical investigation of the fracture scaling in scratch tests and show that scratching is a fracture dominated process. Validated for paraffin wax, cement paste, Jurassic limestone and steel, we derive a model that provides a quantitative means to relate quantities measured in scratch tests to fracture properties of materials at multiple scales. The scalability of scratching for different probes and depths opens new venues towards miniaturization of our technique, to extract fracture properties of materials at even smaller length scales.

DOI: 10.1103/PhysRevLett.106.204302 PACS numbers: 46.50.+a, 46.25.−y, 46.35.+z, 62.20.D−

Scooping cold butter with a knife [Fig. 1(a)] is a familiar experience. As the knife advances along an initially flat surface, it plows and cuts as small chips emanate in the process, leaving behind a well-defined groove. We regard the scooping of butter as a scratch test, which is probably one of the oldest techniques in the characterization of mechanical material properties. For instance, in 1824, Mohs' hardness scale was introduced as an empirical way to quantify the scratch resistance of minerals [1]. Despite the apparent simplicity of this procedure, a fundamental understanding of the underlying mechanism remains aloof. The challenge lies in the difficulty to predictively rationalize the mechanisms that drive the scratch resistance vis-à-vis the chipping of material [Fig. 1(b)], with the shape and size dependence on the mechanical properties of the material, scratch depth and geometry of the scratch device. Nonetheless, the scratch test remains popular today in many applications involving material characterization, including adhesion properties of coatings [2], damage and wear of metals and polymers [3], strength of rocks [4], and skin biomechanics [5].

Here, we focus on scratching as a fracture process and approach this problem through a combination of well-controlled experiments, scaling analysis, and theory. First, we perform precision tests on paraffin wax, which we regard as a model material. Dimensional analysis enables us to identify the mechanical ingredients involved. We then develop a theoretical framework based on an energetic approach to rationalize the process. Our predictive model is turned into an inverse application to determine the fracture toughness for a wide range of materials, cutter-blade geometries, and length scales.

A representative photograph of our experimental setup is presented in Fig. 1(b) and the corresponding schematic diagram of the simplified scratch-cutting test geometry in Fig. 1(c1). We consider paraffin wax for its thermal stability, nearly linear elasticity, and brittle mechanical properties. The tensile strength and fracture toughness of paraffin wax were determined by independent standard tests, namely, the strength by uniaxial tension tests on finite plates with a centered hole, $\sigma_0 = 2.03 \pm 0.25$ MPa, and the fracture toughness by 3-point bending tests on notched specimen, $K_c = 0.146 \pm 0.01$ MPa $\sqrt{\text{m}}$. A paraffin block (dimensions $3.4 \times 5.7 \times 22$ cm) was clamped at its lateral sides, set on a linear stage and moved at constant velocity against a vertical steel cutter blade at depth d (measured from the block's top surface). This blade of rectangular cross section (6.35 mm thick and w wide) was held by a rigid frame that ensured a constant depth and a zero back-rake angle during the test. The values of w and d were

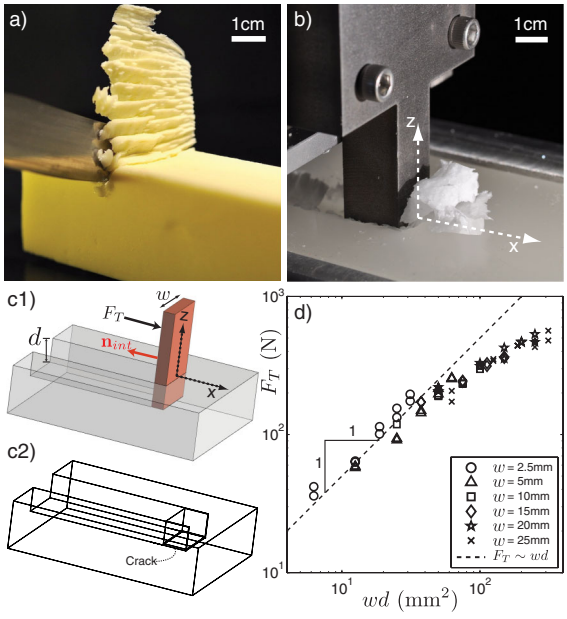

FIG. 1 (color online). (a) Scooping of butter with a knife. (b) Chips formation during the scratch test on paraffin wax. (c1) Schematic diagram of the scratch tests. (c2) Contour surface used in the J integral. (d) Tangential force, F_T, versus projected area of the blade wd. A total number of 55 tests was carried out on paraffin wax with six different scratch widths, $2.5 \leq w \leq 25$ mm, that were operated at five different depths, $2.5 \leq d \leq 12.5$ mm.

varied such that their aspect ratio was in the range $0.2 \leq w/d \leq 10$. For each test, the horizontal and vertical forces generated, F_T and F_V, respectively, were recorded using load cells. In Fig. 1(d) we plot the dependence of the average of F_T as a function of the blade's projected contact area wd. For low values, F_T scales linearly with wd which is significant of a strength process, in which the stress is limited by a threshold value that is the strength of the material, which is proportional to the slope of the curve $F_T(wd)$. However, for higher values of wd, deviations from this linear scaling are attributable to the fracture nature of the problem.

We start by rationalizing the problem through a dimensional analysis of the quantities involved. Neglecting rate and thermal effects, we find that,

$$\frac{F_T}{K_c w\sqrt{d}} = \Pi\left(\frac{w}{(K_c/\sigma_0)^2}, \frac{E}{\sigma_0}, \frac{w}{d}\right), \tag{1}$$

where K_c is the fracture toughness, σ_0 the material strength and E the Young's modulus. The quantity $(K_c/\sigma_0)^2$ has dimensions of length, and is characteristic (within a multiplying factor) of the size of the fracture process zone (FPZ) [6]. In Fig. 2 we reanalyze the original data [Fig. 1(b)], after making use of Eq. (1) to scale the results, and present the dependence of the normalized scratch force, $F_T/(K_c w\sqrt{d})$ versus w/d. Remarkably, the results for all different scratch widths and depths collapse onto a characteristic curve which converges for, $w/d > 2$, to a horizontal asymptote of approximately $\sqrt{2}$. In this domain, the width-to-FPZ ratio is $w/r_p \gg 1$, where the characteristic FPZ size is determined to be $r_p = (\pi/8)(K_c/\sigma_0)^2 = 2.0$ mm, which indicates the validity of applying linear elastic fracture mechanics (LEFM) to our problem. Stress concentration at the blade edges for low w/d may entail plastic dissipation, which is why the experimental values converge to $\sqrt{2}$ for large width-to-depth ratios reminiscent of a fracture process.

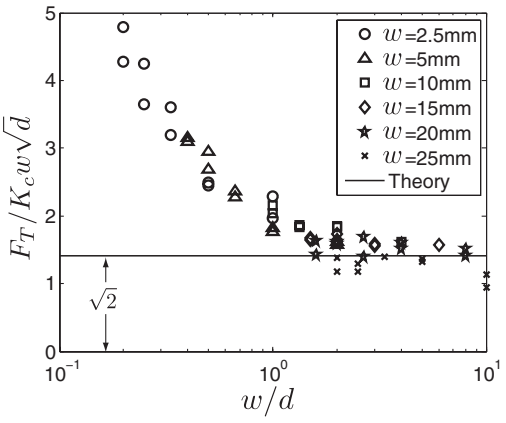

FIG. 2. Fracture scaling of the scratch tests on paraffin wax for blades with $2.5 \leq w \leq 25$ mm and $2.5 \leq d \leq 12.5$ mm. Same raw data as in Fig. 1(d). The solid horizontal line is located at $\sqrt{2}$.

We proceed by developing a quantitative theoretical framework that explains this fracture behavior. The aim is to thereby be able to determine the fracture toughness K_c from the measured tangential force, F_T, the scratch width, w, and scratch depth, d.

Consider a linear elastic fracture process, in the simplified geometry illustrated in Fig. 1(c1). The spontaneous change in potential energy of the system, E_{pot}, is due to the creation of a new fracture surface $\Gamma = p\ell$, where p is the perimeter edge of the cutter blade, defining the crack tip geometry, and ℓ is the crack length. The energy release rate, G, is the thermodynamic driving force of crack propagation, and can be found from the relation,

$$\frac{dE_{\text{pot}}}{dt} = \frac{\partial E_{\text{pot}}}{\partial \Gamma}\dot{\Gamma} = -G\, p\dot{\ell}. \tag{2}$$

For planar crack growth, and within the framework of LEFM, the energy release rate can be estimated using a contour integral procedure, known as the J integral [7,8]. The fundamental idea of this method is to estimate the change in potential energy during a fracture process from the perspective of an observer attached to a propagating crack tip. Under displacement control, this observer witnesses two sources in the change of potential energy: one due to the change in free energy density, ψ, in a material volume, V, enclosing the crack tip; the other due to the energy release that is convectively transported at a speed $\mathbf{V}\cdot\mathbf{n} = -\dot{\ell}n_x$ past the (fixed) observer:

$$\frac{dE_{\text{pot}}}{dt} = \int_V \frac{\partial \psi}{\partial t} dV - \int_A \psi \dot{\ell} n_x \, dA, \tag{3}$$

where A is the closed boundary of V, $\mathbf{n}$ the outward unit normal to A, and $n_x = \mathbf{n}\cdot\mathbf{e}_x$. Developing the volume integral into a surface integral [9] for a linear elastic material, for which $\psi = \frac{1}{2}\sigma_{ij}u_{i,j}$ (σ_{ij} is the stress tensor and $u_{i,j}$ is the displacement gradient), and then comparing Eqs. (2) and (3), yields the energy release rate,

$$G = \frac{1}{p}\int_A \left(\psi n_x - t_i \frac{\partial u_i}{\partial x}\right) dA, \tag{4}$$

where $t_i = \sigma_{ij}n_i$ are surface tractions. Compared to the classical form of the J integral [8], in which the fracture perimeter coincides with the fracture width, $dA = pds$, we choose to consider a difference between these lengths, in order to later extend the technique to other scratch geometries. We hypothesize the existence of crack planes surrounding the blade and choose a closed volume that includes [Fig. 1(c2)] (i) the blade-material interface, the stress-free surface at the top ($n_x = 0; t_i = 0$), (ii) the (stress-free) fracture surfaces in prolongation of the scratch probe surface ($n_x = 0; t_i = 0$), and (iii) closing material surfaces far removed from the surfaces ($\psi = 0; u_{i,x} = 0$). Physically, the energy release so defined is associated with the energy stored, prior to chipping, into a material domain in front of the scratch blade.

For the case of a rectangular blade ($n_x = -1$) of width w, the generated fracture surface is $\Gamma = (w + 2d)\ell$. Noting that $t_i = \sigma_{ij}n_i = -\sigma_{xx}\varepsilon_x$, $\sigma_{xx} = -F_T/(wd)$; $\psi = \frac{1}{2}\sigma_{xx}\varepsilon_{xx} = \kappa\sigma_{xx}^2/(2E)$; $u_{x,x} = \kappa\sigma_{xx}/E$ (where $\kappa = 1$ for unconfined and $\kappa = 1 - \nu^2$ for confined stress state applications) and $dS = wdz$, we readily obtain, $G = \kappa F_T^2/[2Ew^2d(1 + 2d/w)]$. As the scratch probe advances, fracture surfaces are generated along the probe's bottom and lateral surfaces. In the process, a fracture energy G_c is released, which can be related to the fracture toughness as $G_c = \kappa K_c^2/E$, [10]. Expressed in terms of the dimensionless expression of Eq. (1), the fracture propagation criterion therefore reads as,

$$\frac{F_T}{K_c w\sqrt{d}} = \sqrt{2}\left(1 + 2\frac{d}{w}\right)^{1/2}. \quad (5)$$

For large enough w/d ratios, Eq. (5) quantitatively confirms the fracture scaling of Eq. (1) and accurately describes the asymptotic value of $\sqrt{2}$ in the experimental results plotted in Fig. 2, for the scratch tests with paraffin. This opens the path for using the fracture criterion of Eq. (5) in an inverse application to determine the fracture toughness, K_c, for large values of w/d.

We now explore the generality of our scratch fracture model, by predicting the fracture toughness in different experimental assays for two additional blade geometries, at different length scales: (i) an inclined rectangular cutter blade and (ii) a conical scratch device.

In the first case, an inclined blade (back-rake angle θ and out-of-plane width w) is held at a depth d by a vertical force F_V [Fig. 3(a), inset]. In contrast to the previous straight blade, F_V is applied through the inclined surface and needs to be considered in the calculation. The classical J integral ($w = p$) evaluated in this configuration [11] yields $J = \kappa F_{eq}^2/(2Ew^2d)$ and $F_{eq} = (F_T^2 + \frac{3}{5}F_V^2)^{1/2}$. Noting that the projected perimeter of the fracture surface is now $p = w + 2d$, and correcting for w/p, i.e. $G = (w/p)J$, we obtain a fracture criterion analogous to Eq. (5),

$$\frac{F_{eq}}{K_c w\sqrt{d}} = \sqrt{2}\left(1 + 2\frac{d}{w}\right)^{1/2}, \quad (6)$$

where the tangential force is replaced by a force, F_{eq}, that accounts for both F_T and F_V and drives the fracture process over the inclined blade-material interface.

In Fig. 3 we apply this new fracture criterion to the experimental test of two materials—a cement paste and a Jurassic limestone—using the inclined blade geometry (15° back-rake angle). In Figs. 3(a) and 3(c) we plot F_{eq} vs $w\sqrt{2d}$, over a scratch path of 3.5 cm. Two observations deserve particular attention. First, the straight-line fits confirm the linearity between F_{eq} and $w\sqrt{2d}$ for each scratch width series. Moreover, the slope, which is representative for large values of w/d of the fracture toughness, decreases with the increase of the scratch width. In the linear fit of the data, we admit an offset value [Fig. 3(c), inset], which can be attributed to the highly localized plastic deformation at the contact of the indenter with the material. In Figs. 3(b) and 3(d) we explore the same results, in terms of $F_{eq}/(w\sqrt{2d})$ vs w/d. As in the previous case for paraffin, $F_{eq}/(w\sqrt{2d})$ converges with w/d to a constant value that is representative of the fracture toughness. The mean value for cement paste toughness of $K_c = 0.66 \pm 0.05$ MPa $\sqrt{\text{m}}$ obtained from averaging $F_{eq}/w\sqrt{2d}$ values for $w/d > 10$ is indeed in excellent agreement with reported fracture toughness values obtained by notched three-point bending tests for large specimen, $K_c = 0.67$ MPa $\sqrt{\text{m}}$ [12], or by means of extrapolation techniques that avoid interference with specimen size, $K_c = 0.65$ MPa $\sqrt{\text{m}}$ [13]. We have also successfully employed this technique for other geomaterials, including sandstone and cemented siltstone.

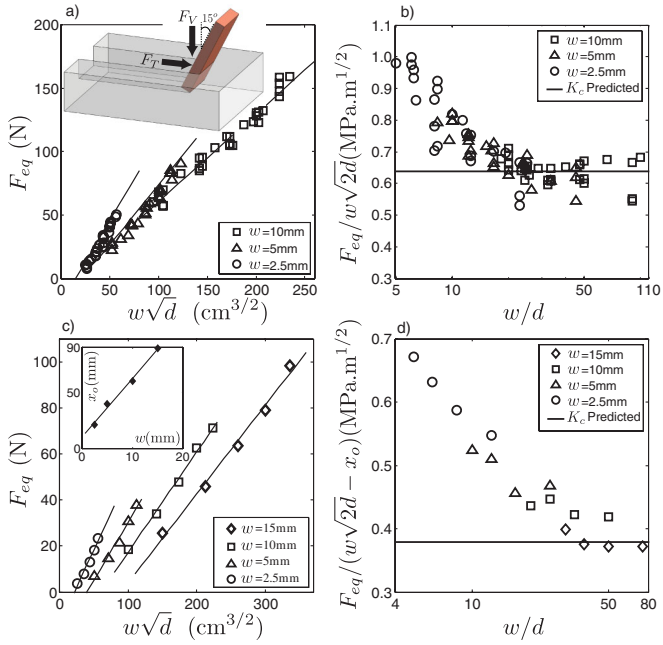

FIG. 3 (color online). Fracture scaling of the scratch tests for cement paste and Jurassic limestone. (a), (b) Cement Paste. (c), (d) Jurassic limestone. The back-rake angle in all tests was 15°—inset (a). Three test series for cement paste and four series for limestone were conducted with scratch width, $w = 2.5$ mm, 5 mm, 10 mm and 15 mm, and with scratch depth $d = 0.1$–0.6 mm, spanning almost 2 orders of magnitude of w/d, from 5 to 100.

Finally, we consider a conical scratch device [schematic diagram in Fig. 4(a)], which is routinely used in micro- and nanoscratch applications [14]. In these tests, the protocol typically consists of linearly increasing the vertical force, F_V, along the scratch path [solid line in Fig. 4(b)], resulting in an increase of both the scratch depth and groove size. In parallel, the tangential force, F_T is measured [dashed line in Fig. 4(b)]. A representative top view of the resulting scratch path is presented in Fig. 4(c).

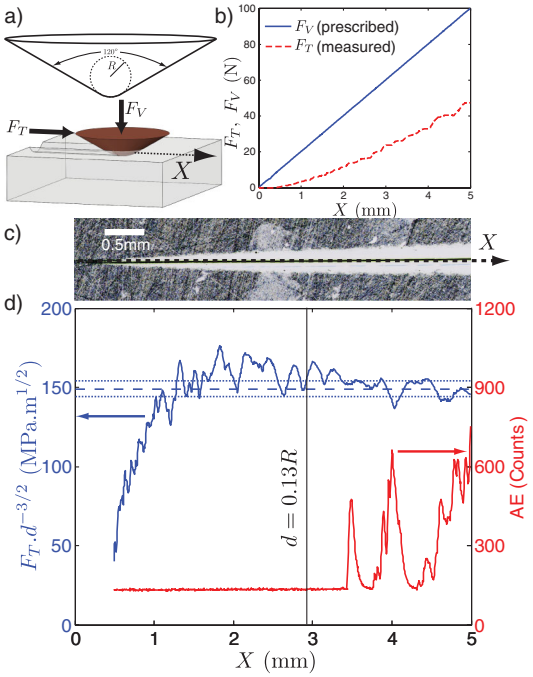

FIG. 4 (color online). (a) Schematic diagram of the conical indenter; see text for the geometrical details of the probe. (b) Prescribed vertical and measured tangential forces during the scratch test. The vertical force F_V is linearly increased and the resulting tangential force F_T is recorded. (c) Photograph of the residual groove obtained after the scratch test, where the scratched region appears as light gray. (d) Fracture scaling of the microscratch test (left axis) and acoustic emission associated with the fracture process (right axis). Dashed and dotted lines represent mean value ± st. dev. for the conical probe region.

To simplify the analysis, the vertical force is assumed to be entirely submitted through the contact area into the material. To first approximation, we assume a constant uniaxial stress $\sigma_{xx} = -F_T/A$ over the projected (load bearing) contact area $A = \int_{(S)} n_x dS$ so that $t_i = \sigma_{ij} n_i = -\sigma_{xx} n_x$. Following the same procedure for the contour integral of the energy release rate, the general form for the fracture criterion yields, $F_T/\sqrt{2pA} = K_c$. For a conical scratch device of half-apex angle θ, perimeter $p = 2d/\cos\theta$ and projected contact area $A = d^2 \tan\theta$, we obtain:

$$\frac{F_T}{K_c d^{3/2}} = 2\sqrt{\frac{\tan\theta}{\cos\theta}}. \tag{7}$$

To validate this fracture scaling, we carried out scratch tests on steel with a Rockwell diamond probe. This conical probe of half-apex angle $\theta = 60°$ ends in a hemispherical tip with mean radius $R = 200$ μm, which transitions from the sphere to the cone at $d/R = 0.132$ [see schematic in Fig. 4(a)]. In Fig. 4(d) we present the scaling of $F_T/d^{3/2}$ vs the scratch path, X, for a microscratch test on steel. In this experiments, F_V is linearly imposed from zero to 100 N [Fig. 4(b)] resulting in a variable depth up to 47 μm and a residual groove along a 5 mm scratch path [Fig. 4(c)]. The most important feature that emerges from the data shown in Fig. 4(d) is that $F_T/d^{3/2}$ converges towards a straight line in the region of the conical probe, where acoustic emissions [15] provide strong evidence that a fracture process is indeed at play. Through Eq. (7), we determine the fracture toughness of the material at microscales, $K_c = 40 \pm 0.2$ MPa $\sqrt{\text{m}}$, a value that is consistent with typical macrotoughness values for steel, $K_c = 50$ MPa $\sqrt{\text{m}}$ [16].

In summary, we have uncovered that scratching is a fracture dominated process. The model we have proposed and validated through well-controlled experiments provides a readily applicable methodology to determine fracture toughness of materials. The scalability of our approach opens new venues towards further miniaturization of this technique, to extract fracture properties of materials at even smaller length scales.

We are grateful to B. Lecampion (Schlumberger) and C. Germay (Epslog Engineering) for the data on cement paste and Jurassic limestone, to N. X. Randall for making available the CSM Instruments Revetest Testing System [14], and to J. Germaine, S. Rudolph, H. Ryan and J. Miller for technical assistance.

*To whom all correspondence should be addressed.
ulm@mit.edu

[1] D. T. Tabor, Proc. Phys. Soc. London Sect. B **67**, 249 (1954); M. E. Broz, R. F. Cook, and D. L. Whitney, Am. Mineral. **91**, 135 (2006).
[2] H. Ollendorff and D. Schneider, Surf. Coat. Technol. **113**, 86 (1999).
[3] F. Wredenberg and P. L. Larsson, Wear **266**, 76 (2009).
[4] G. Schei *et al.*, SPE Journal, doi:10.2118/63255-MS (2000).
[5] J. G. Thacker *et al.*, Clin. Plast. Surg. **4**, 167 (1977).
[6] G. I. Barenblatt, Adv. Appl. Mech. **7**, 55 (1962).
[7] G. P. Cherepanov, Appl. Math. Mech. **31**, 503 (1967).
[8] J. R. Rice, J. Appl. Mech. **35**, 379 (1968).
[9] The divergence theorem allows a change of the volume integral in Eq. (3) into a surface integral and we also make use of the fact that in a displacement-controlled fracture test the displacement rate seen by the moving observer is equal to $u_{i,t} = \dot{\ell} u_{i,x}$.
[10] A. A. Griffith, Phil. Trans. R. Soc. A **221**, 163 (1921).
[11] A-T. Akono and F-J. Ulm, Eng. Fract. Mech. **78**, 334 (2011).
[12] B. Cotterell and Y. W. Mai, J. Mater. Sci. **22**, 2734 (1987).
[13] X. Wu and F. Wittman, Eng. Fract. Mech. **65**, 209 (2000).
[14] N. X. Randall *et al.*, Surf. Coat. Technol. **137**, 146 (2001).
[15] T. R. Wilshaw and R. Rothwell, Nature (London) **229**, 155 (1971).
[16] W. T. Matthews, *Plane Strain Fracture Toughness (KIc) Data Handbook for Metals, AMMRC MS73-6* (U. S. Army Materials and Mechanics Research Center, Watertown, MA, 1973).